Human Molecular Genetics, 2011, Vol. 20, No. 21 ***4209–4223***
doi:10.1093/hmg/ddr348
Advance Access published on August 9, 2011

LRRK2 protein levels are determined by kinase function and are crucial for kidney and lung homeostasis in mice

Martin C. Herzig[1], Carine Kolly[5], Elke Persohn[5], Diethilde Theil[5], Tatjana Schweizer[1], Thomas Hafner[1], Christine Stemmelen[1], Thomas J. Troxler[2], Peter Schmid[1], Simone Danner[1], Christian R. Schnell[3], Matthias Mueller[4], Bernd Kinzel[4], Armelle Grevot[5], Federico Bolognani[5], Martina Stirn[5], Rainer R. Kuhn[1], Klemens Kaupmann[1], P. Herman van der Putten[1], Giorgio Rovelli[1] and Derya R. Shimshek[1,*]

[1]Department of Neuroscience, [2]Global Discovery Chemistry, [3]Department of Oncology, [4]Developmental and Molecular Pathways and [5]Preclinical Safety, Novartis Institutes for BioMedical Research, Novartis Pharma AG, CH-4002 Basel, Switzerland

Received June 20, 2011; Revised and Accepted August 4, 2011

Mutations in leucine-rich repeat kinase 2 (LRRK2) cause late-onset Parkinson's disease (PD), but the underlying pathophysiological mechanisms and the normal function of this large multidomain protein remain speculative. To address the role of this protein *in vivo*, we generated three different LRRK2 mutant mouse lines. Mice completely lacking the LRRK2 protein (knock-out, KO) showed an early-onset (age 6 weeks) marked increase in number and size of secondary lysosomes in kidney proximal tubule cells and lamellar bodies in lung type II cells. Mice expressing a LRRK2 kinase-dead (KD) mutant from the endogenous locus displayed similar early-onset pathophysiological changes in kidney but not lung. KD mutants had dramatically reduced full-length LRRK2 protein levels in the kidney and this genetic effect was mimicked pharmacologically in wild-type mice treated with a LRRK2-selective kinase inhibitor. Knock-in (KI) mice expressing the G2019S PD-associated mutation that increases LRRK2 kinase activity showed none of the LRRK2 protein level and histopathological changes observed in KD and KO mice. The autophagy marker LC3 remained unchanged but kidney mTOR and TCS2 protein levels decreased in KD and increased in KO and KI mice. Unexpectedly, KO and KI mice suffered from diastolic hypertension opposed to normal blood pressure in KD mice. Our findings demonstrate a role for LRRK2 in kidney and lung physiology and further show that LRRK2 kinase function affects LRRK2 protein steady-state levels thereby altering putative scaffold/GTPase activity. These novel aspects of peripheral LRRK2 biology critically impact ongoing attempts to develop LRRK2 selective kinase inhibitors as therapeutics for PD.

INTRODUCTION

Parkinson's disease (PD) is the most prevalent neurodegenerative movement disorder with different genetic and environmental etiologies and no existing cure. Clinical motor features include bradykinesia, rigidity and resting tremor, but a variety of non-motor symptoms are known, some of which even precede the appearance of motor symptoms. The main neuropathological hallmark underlying the clinical motor features is the loss of dopaminergic (DA) neurons in the substantia nigra pars compacta. α-synuclein-containing Lewy structures reminiscent of a specific proteinopathy are found in surviving DA but also many other central and peripheral neurons including those in the gastrointestinal nervous

*To whom correspondence should be addressed. Tel: +41 616962388; Fax: +41 616912925; Email: derya.shimshek@novartis.com

system, and may contribute to the spectrum of non-motor symptoms in PD patients (1). Human genetics has defined several mutations in the leucine-rich repeat kinase 2 (*LRRK2*) gene as a cause of late-onset autosomal dominant PD that is clinically indistinguishable from idiopathic PD. LRRK2 mutations account for ~5% of familial and 1–2% of sporadic PD cases and one mutation, G2019S, is most prevalent (2–7). Although genetics has unequivocally established a causal role for LRRK2 mutations in PD, the underlying molecular pathophysiology is not understood (8). Polymorphisms in the *LRRK2* gene have also been associated with disorders including Crohn's disease (9) and cancer (10). *In vitro*, LRRK2 displays kinase activity on itself and artificial substrates (11). Physiological substrates have remained elusive. Nonetheless, the G2019S mutation is located in the kinase domain and increases LRRK2 kinase activity (12,13) and toxicity (14–17). Altogether, these findings provide a rationale for finding and developing LRRK2-selective kinase inhibitors in PD. LRRK2 also has a GTPase as well as a number of protein–protein interaction domains. Which domain and function of LRRK2 exerts the protein's main up- and/or downstream pathway effector function remains to be clarified (11). Mouse and human LRRK2 proteins share 86.7% amino acid identity (www.ncbi.nlm.nih.gov/homologene). In the brain, LRRK2 is expressed in the nigrostriatal pathway as relevant to PD, but is not restricted to this pathway. In addition, several peripheral organs and cell types express LRRK2 including kidney, lung and B cells suggesting that LRRK2 mutations may impact physiological processes and exert disease-relevant roles outside the nervous system (9,10). Elucidating the function of the kinase, GTPase and protein–protein interaction domains of LRRK2, and investigating its role outside the brain will facilitate a better understanding of LRRK2-associated PD and promote the development of LRRK2 bioassays, biomarkers and therapeutic strategies. Here we generated LRRK2 mutant mouse lines to investigate fundamental aspects of LRRK2 biology *in vivo* that specifically relate to its role as a kinase.

RESULTS

Kidney and lung pathology in LRRK2 mutant mice

To determine how kinase function contributes to roles of LRRK2 *in vivo*, we generated mutant mice (Supplementary Material, Fig. S1) carrying either a kinase-inactivating point mutation D1994S (kinase-dead, KD, Supplementary Material, Fig. S2) or the kinase-enhancing G2019S pathogenic mutation (knock-in, KI) that genocopies the human G2019S PD-causing mutation. Both mutations occur in coding exon 41 of the murine *LRRK2* gene. To distinguish LRRK2 kinase from potential scaffolding functions of LRRK2, we generated mice lacking LRRK2 completely (knock-out, KO).

In wild-type (WT) mice, the LRRK2 protein is highly expressed in the kidney (see below and Fig. 5B). Remarkably, both KO and KD but not KI and WT mice developed dark kidneys (Fig. 1A–C), thus confirming an earlier report on KO mice (18) and extending this finding to KD but not KI mice even at an age of 26 months. Kidney weight significantly increased in adult homozygous KD males, but remained unchanged in heterozygous KD males and in 3-month-old homozygous KD females (Fig. 1A). Histological examination of KD mouse kidneys at ages between 1.5 and up to 8 months and from two genetic backgrounds (BALB/c and C57BL/6) all showed localized microvacuolization manifested as an accumulation of many small isometric vacuoles in epithelial cells of the proximal tubules in both cortex and outer medulla (Fig. 1A and data not shown). Starting at the age of 8 months, vacuolated epithelial cells showed in addition a multifocal accumulation of granular, yellow–brown autofluorescent pigment reminiscent of lipofuscin (Supplementary Material, Fig. S3A) and an indicator for cellular aging (19,20). Like KD mice, KO mice also showed a male gender-specific increase in kidney weight starting around 5 months of age that persisted life-long but showed no significant incremental increase with age (Fig. 1C and Supplementary Material, Fig. S3D). Darkening of KO kidneys, however, occurred independent of sex starting around the age of 5 months (Fig. 1C). It did not occur in heterozygous KO mice (data not shown). KO like KD kidneys started to show diffuse microvesicular vacuolation in proximal tubule epithelial cells of the cortex and outer medulla as early as 6 weeks after birth (Fig. 1C). With age, microvacuoles became larger and more-and-more tubules were affected. At age of 5 months, KO like KD kidneys showed tubular dilatation and increased intracellular deposition of lipofuscin. In 8-month-old mice, KO but not KI kidneys showed tubular degeneration and extracellular deposition of lipofuscin (Fig. 1C and Supplementary Material, Fig. S3B and C). Interestingly, these LRRK2-specific pathophysiological changes in KO kidneys did not prevent or accelerate grossly other mouse species-specific age-related kidney histopathological changes that are typically observed in WT (and also KI) mice, such as glomerulonephropathy and tubulointerstitial nephritis (data not shown). We also found no histopathological evidence of genotype-related cell loss in kidneys of KO mice (data not shown).

To determine whether the LRRK2-specific changes impaired kidney function we performed urinalysis. Twenty-two-month-old KO females (Fig. 1D) and 18-month-old KO males (Supplementary Material, Fig. S3F) developed proteinuria which was not yet observed at age 5 months (Fig. 1D) or in 20-month-old KI males (Supplementary Material, Fig. S3F).

Microvacuolation as a result of LRRK2 ablation was also seen in lung tissue (Fig. 1E) where LRRK2 is expressed (see below and Fig. 5B). Here, they were restricted to a subset of large epithelial cells, classified as type II pneumocytes, and located within the alveolar-septal walls. These cells stained positive for Mucin-1 (data not shown). Type II pneumocytes are proliferating epithelial cells that produce and secrete phospholipid surfactant (21,22). Like in the kidney, also in the lung the changes were apparent already at the age of 1.5 months (Fig. 1E). They did not affect lung weight (Supplementary Material, Fig. S3E). The morphology of the microvacuoles in lung cells was similar to those observed in kidney tubular cells. Neither KD nor KI mice showed similar changes in the lung (Supplementary Material, Fig. S4 and data not shown). Other organs in KO mice including the brain and spleen which both have high levels of LRRK2 in WT animals (Fig. 5B), and organs such as the heart and liver showed no LRRK2 genotype-related histopathology

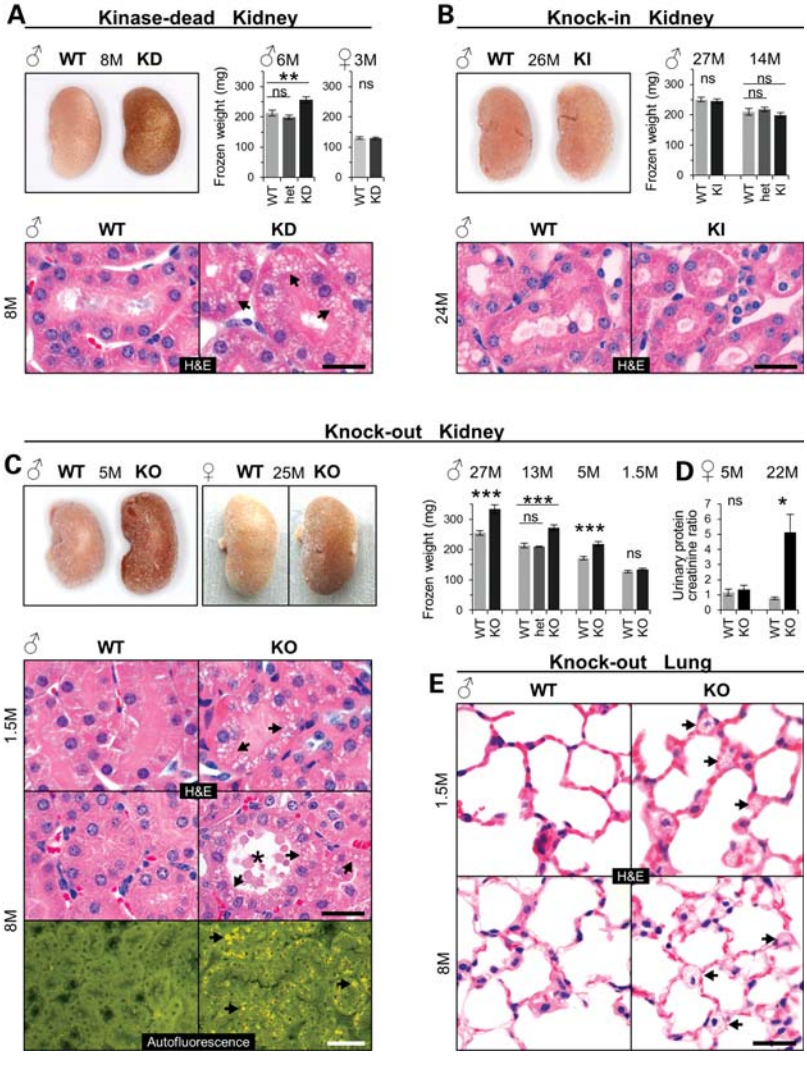

Figure 1. Kidney and lung pathology in LRRK2 mutant mice. (**A**–**C**) Gross appearance, weights of fresh-frozen kidneys and histology of kidney sections stained with H&E in KD (A), KI (B) and KO mouse kidney (C) or showing autofluorescent material deposited in KO mice (C). Arrows point to microvacuoles (H&E) and pigment deposits (autofluorescence). Frozen kidney weights (average of left and right kidney): $n = 5–16$ per group and genotype. (**D**) Analysis of proteinuria in female KO and WT mice (5 months old: $n = 12$ per genotype and 22-month-old mice: $n = 5–6$ per genotype). Urinary protein content was normalized to creatinine levels. (**E**) H&E-stained lung sections from male KO and WT mice. Arrows point to microvacuoles. Age in months (M) and gender are indicated. Bars in graphs show means and error bars represent SEM. Asterisks indicate significance determined by two-tailed *t*-test, $^{*}P < 0.05$, $^{**}P < 0.01$, $^{***}P < 0.001$, ns: not significant. Scale bars: 25 μm (black), 50 μm (white).

even in 26-month-old mice (data not shown). Altogether, these histopathological findings demonstrate that LRRK2 serves homeostatic roles in the kidney and lung and that, when perturbed, result in pronounced microvacuolation of select cell types. Whether these changes are cell autonomously linked to LRRK2 dysfunction and/or the result of compensatory mechanisms triggered because of LRRK2-dependent dysfunction elsewhere in these tissues cannot unequivocally be demonstrated at this point.

Alterations in proximal tubule secondary lysosomes and lung type II pneumocyte lamellar bodies

To further characterize the microvacuoles, we first performed immunohistochemistry for lysosome-associated membrane protein 1 (LAMP1), a marker of late endosomes and lysosomes. In 6-week-old KO kidneys, tubules showed increased LAMP1 staining. The LAMP1-positive structures were enlarged and redistributed from an otherwise apical localization in WT tubules to a perinuclear distribution in KO tubules (Fig. 2A). Similar results were obtained in KD kidneys of 9-month-old mice, analyzed with LAMP2 immunohistochemistry (data not shown).

For a more detailed characterization, we performed electron microscopic (EM) analysis (Fig. 2B). Kidneys of 2-month-old KO mice revealed an increase in the number and size of secondary lysosomes in some but not all proximal tubules. At age 6 months, most of the KO kidney proximal tubules contained enlarged and increased numbers of secondary lysosomes with typical stacked, whorled membranes, lipid and fine granular electron dense homogenous material. The fraction of the whorled membranes was substantially increased in KO when

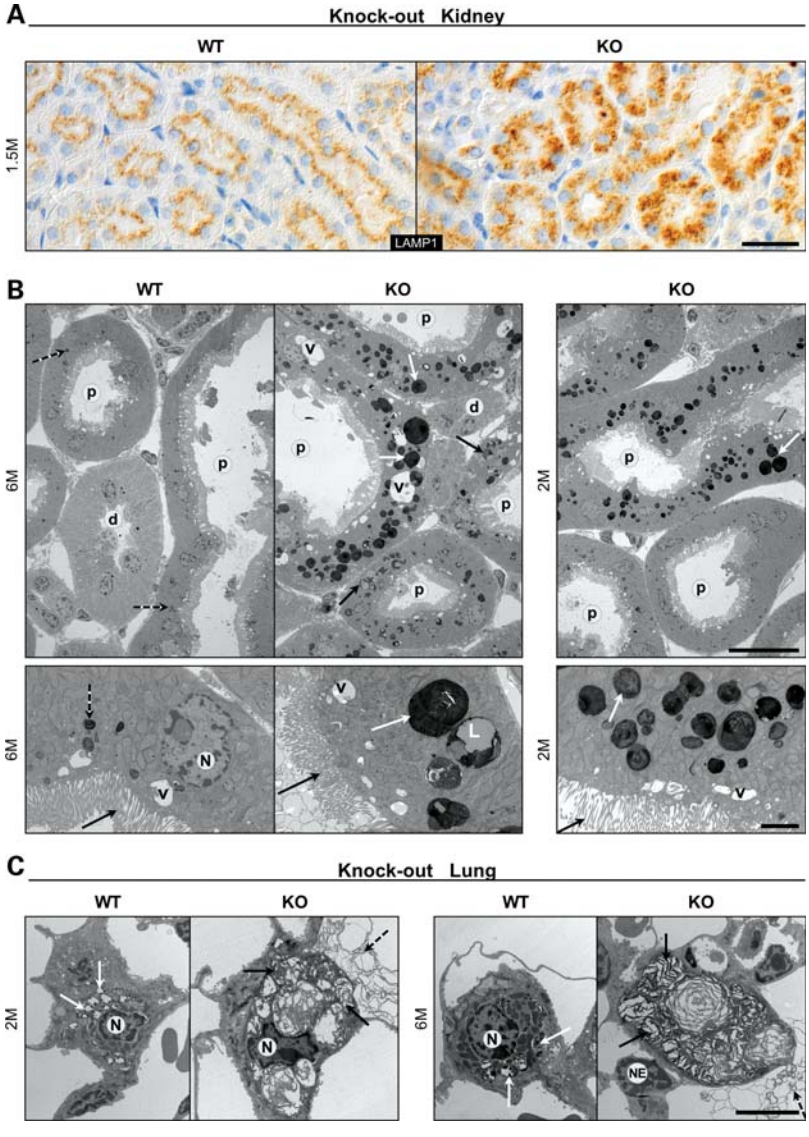

Figure 2. Accumulation of secondary lysosomes in kidney proximal tubule epithelial cells and lamellar bodies in lung type II pneumocytes. (**A**) Light microscopy showing LAMP1 immunostaining (brown DAB staining) in kidney tubules of 1.5-month-old WT and KO mice. Electron microscopy showing kidney cortical proximal (p) and distal (d) tubules (**B**) and lung alveolar type II cells (**C**) from 6-month-old WT and 6- or 2-month-old KO mice. Male mice were used for analysis. (B, upper panel) Normal secondary lysosomes (dashed arrows) and enlarged secondary lysosomes with electron dense material (white arrows) and lipids (black arrows). V: enlarged apical vacuoles (phagosomes). (B: lower panel) Brush border microvilli (black arrows), normal secondary lysosomes (dashed arrows), enlarged secondary lysosomes with whorled membranes (white arrows) and lipids (L). V: apical vacuoles (phagosomes), N: cell nucleus. (C) Type II pneumocyte with normal lamellar bodies in WT lungs (white arrows) and enlarged lamellar bodies in KO lungs (black arrows). Dashed arrows indicate the surfactant. N: type II pneumocyte cell nuclei, NE: endothelial cell nucleus. Scale bars: 50 μm (A), 20 μm (B, upper panel), 2.5 μm (B, lower panel), 5 μm (C).

compared with WT kidneys, indicating an accumulation of phospholipid membranes. Further, the number of lysosomes with lipid and fine granular electron dense material as well as the number and size of apical vacuoles (phagosomes which contained cellular debris) was increased. Other cellular organelles in proximal tubule epithelial cells, such as mitochondria and peroxisomes, did not show morphological alterations when compared with the WT. Distal tubules and glomeruli showed essentially no changes when compared with WT mice (data not shown).

EM studies on lung tissue from 2- and 6-month-old KO mice revealed morphological alterations in type II pneumocytes (Fig. 2C). Lamellar bodies were increased in number and size showing little or no age-dependent differences. These lysosome-related organelles store and secrete pulmonary surfactant and their lamellae are composed mainly of phospholipids (23). Like in the kidney, no obvious changes were apparent in other organelles inside type II cells like mitochondria or other lung cell types (data not shown).

These findings demonstrate that both LRRK2 KO and KD mutants cause specific changes in lysosomal homeostasis in kidney tubule epithelial cells, and the KO mutant also alters homeostasis of lamellar bodies in lung type II pneumocytes. Noteworthy, and in contrast to what has been reported (18),

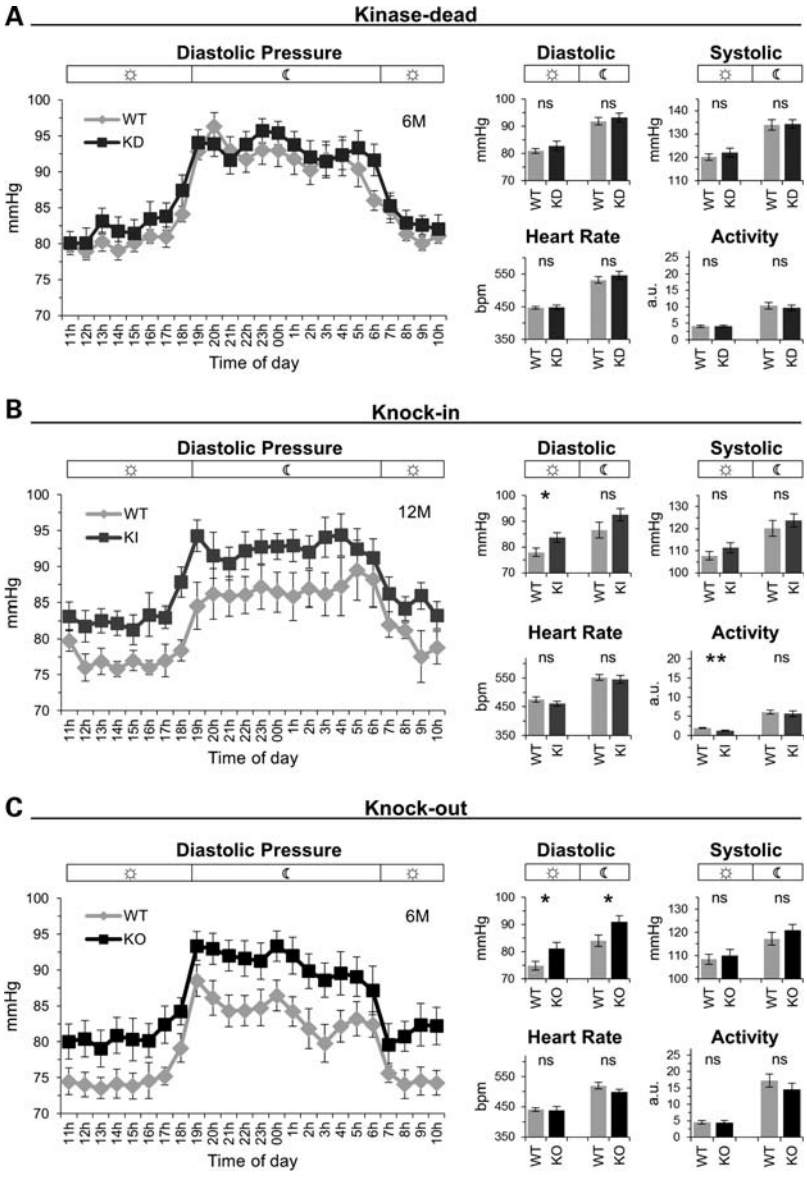

Figure 3. Diastolic hypertension in KO and KI, but not in KD mice. (**A**–**C**) Line graphs showing 24 h measurements of the diastolic blood pressure in 1 h intervals and bar graphs showing the day/night-time mean for diastolic, systolic blood pressure, heart rate and activity for KD (WT: $n = 8$, KD: $n = 9$) (A), KI (WT: $n = 7$, KI: $n = 7$) (B), KO (WT: $n = 8$, KO: $n = 8$) mice (C). Night-time from 19 to 6 h. Bars in graphs show means and error bars represent SEM. Asterisks indicate significance determined by two-tailed *t*-test, $^{*}P < 0.05$, $^{**}P < 0.01$, ns: not significant.

we found no evidence of α-synuclein accumulation in KO kidneys (Supplementary Material, Fig. S5).

Blood pressure changes in LRRK2 mutant mice

The kidneys play a central role in salt handling and many genes that alter this process cause hypo- or hypertension (24–26). Therefore, we determined whether LRRK2 mutations and/or the KO and KD but not KI associated kidney abnormalities influenced blood pressure. Telemetric recordings revealed a moderate but significant increase in diastolic blood pressure in KO and KI but not in KD mice (Fig. 3). Notably, we observed no change in vascular responses of isolated thoraxial and abdominal aorta from KO and KI mice (data not shown). Heart rate (Fig. 3) and weight (data not shown) were not affected. Systolic blood pressure was not altered (Fig. 3). As the KD and KO but not the KI mutants showed similar histopathological findings in the kidney, whereas only KO and KI but not the KD mutants showed changes in blood pressure, the latter seem to occur independent of the histopathological alterations in the kidney. Furthermore, LRRK2 effects on diastolic blood pressure are likely dependent on LRRK2 protein expression but not on its kinase function.

Kidney Akt/mTOR/4E-BP1 pathway changes in LRRK2 mutant mice

LRRK2 has been implicated in autophagy (18,27–29), a process that, when perturbed, could account for an increase

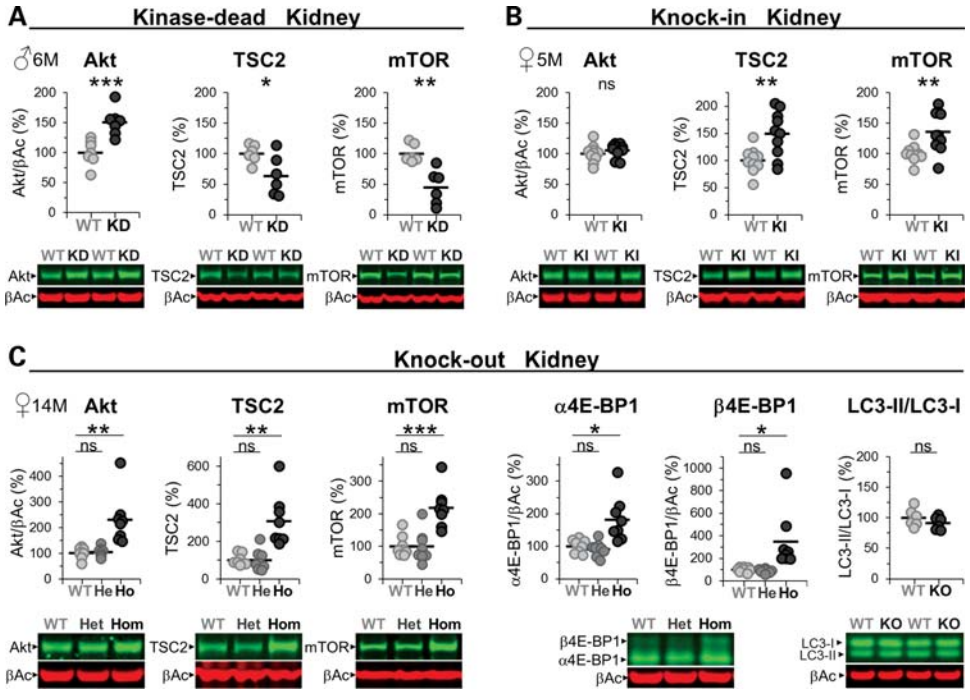

Figure 4. Alterations in Akt/mTOR/4E-BP1 levels in the LRRK2 mutant kidney. (**A**–**C**) Immunoblot quantifications of total kidney lysates (in % normalized to WT) and representative examples thereof from KD (WT, KD: $n = 6–7$) (A), KI (WT, KI: $n = 9–10$) (B) and KO (KO (Ho), heterozygous KO (He) and WT: $n = 6–8$) mice (C). α4E-BP1 represents non- or single-phosphorylated and β4E-BP1 double-phosphorylated 4E-BP1 (C). Asterisks indicate significance determined by two-tailed *t*-test: $^{*}P < 0.05$, $^{**}P < 0.01$, $^{***}P < 0.001$, ns: not significant. Individual mice are shown as circles, the means are indicated as lines. The age in months (M) and gender of the mice are indicated. β-Actin was used as loading control and for Akt and 4E-BP1 normalization.

in the number of microvacuoles in the KO and KD kidney and lung (KO only). However, none of the mutant kidneys showed alterations in LC3I/II levels (Fig. 4C and Supplementary Material, Table S1). Nevertheless, we observed in immunohistochemical analysis an increase of p62 in KO kidneys (Supplementary Material, Fig. S6) as described before (18) which seemed to localize to the secondary lysosomes and thus again implying that lysosomal homeostasis is altered. We did notice changes in mTOR (mammalian target of rapamycin), a central regulator of autophagy (30) and TSC2 levels; reduced in KD but increased in KI and KO mutant kidneys (Fig. 4), but phosphorylation levels of S6(Ser235/236 and Ser240/244) were not changed suggesting no gross changes in the activation state of mTOR (Supplementary Material, Table S1). Akt levels were increased in KD and KO but unchanged in the KI kidney and the phosphorylation levels of the PDK1 site (Thr308) were unchanged (Supplementary Material, Table S1). The levels of 4E-BP1 phosphorylation were, however, increased in KO (Fig. 4C) and KD (Supplementary Material, Table S1) but not KI mice (Supplementary Material, Table S1) which suggest reduced suppression of protein synthesis by 4E-BP1. Note that phosphorylation of 4E-BP1 results in an electrophoretic mobility shift of the protein to higher molecular weight (31). Similar results were obtained in KO and KI kidneys with an anti-phospho-4E-BP1(Thr37/46) antibody (Supplementary Material, Table S1). Gene expression analysis revealed no changes in any of the mRNA levels for Akt, mTOR, S6K, S6 or 4E-BP1 (data not shown) and at the protein level, heterozygous KO mice did not show any alterations (Fig. 4C). Furthermore, these changes seemed kidney-specific and were not observed, for example, in spleen (data not shown). Interestingly, immunoblot analysis also revealed a truncated mTOR protein in the kidney (Supplementary Material, Fig. S7; as well as truncated forms of TSC2 and Akt; data not shown) which levels seemed inversely correlated with those of the full-length mTOR protein in KD and KO but not KI mice (Supplementary Material, Fig. S7). Unlike these changes in older kidneys, 6-week-old kidneys, which appeared grossly normal but already manifested microvacuoles, revealed no changes in the levels of mTOR, Akt or TSC2 (data not shown). Therefore, most of these changes are likely secondary and compensatory.

LRRK2 kinase function is essential for LRRK2 protein stability

Full-length LRRK2 protein levels were similar in organs, including the brain, kidney, lung and spleen (Fig. 5A and B). Different brain regions, like striatum, hippocampus, cortex and cerebellum, expressed similar amounts of the LRRK2 protein, while others (e.g. brainstem) had much lower levels (data not shown). In the kidney, a prominent truncated form of LRRK2 (t1) was detected which was absent in KO (Fig. 5B), reduced to ∼50% in heterozygous KO (Fig. 5C), unchanged in KI mice (Fig. 5D) and present only in much smaller amounts in other organs (Fig. 5B). Notably, homogenization conditions (degree of blockade of phosphatases/proteases) determined the extent and pattern of proteolytic cleavage of LRRK2 (Supplementary Material, Fig. S8), thus

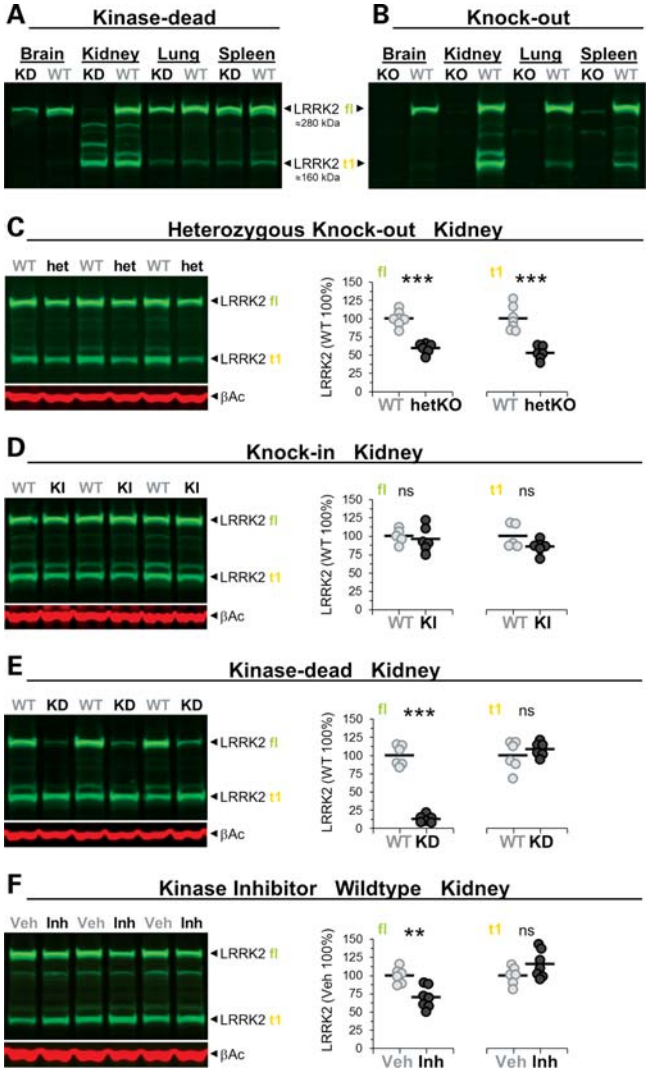

Figure 5. LRRK2 kinase function required for stability of full-length LRRK2 protein. (**A**–**F**) Immunoblots detecting LRRK2 protein in different tissues of adult KD (A) and KO (B) and in the kidney of adult heterozygous KO (het/hetKO) (C), KI (D), KD (E) and kinase inhibitor-treated mice (F). Besides LRRK2 full-length (fl), truncated LRRK2 species were observed mainly in the kidney (most prominent band is indicated as t1). The approximate molecular weight of LRRK2 fl and t1 is indicated. (C–F) Immunoblot quantifications of extracts of total kidney from heterozygous KO (WT, hetKO: $n = 6–7$) (C), KI (WT, KI: $n = 5–6$) (D), KD (WT, KD: $n = 6$) (E) and mice treated with the LRRK2 kinase inhibitor (vehicle, Veh; inhibitor, Inh: $n = 6–7$; 30 mg/kg, p.o., twice daily, 5 days, killed 2 h after last dosing) (F). Shown are quantifications of fl and t1 (in % normalized to WT and vehicle, respectively). Individual mice are shown as circles, means are indicated as lines. Asterisks indicate significance determined by two-tailed *t*-test: $^{**}P < 0.01$, $^{***}P < 0.001$. β-Actin was used as loading control.

highlighting the importance of well-controlled conditions in biochemical experiments regarding LRRK2. To eliminate or minimize artifacts during sample preparation, we inhibited proteases and phosphatases as described under 'additional phosphatase and protease inhibitors' in the Material and Methods section. t1 represents a truncated form of LRRK2 that includes the leucine-rich repeat (LRR) region and the kinase domain as shown by mass spectrometry analysis of pull-down material with LRRK2-inhibitor coated beads (data not shown). In KD mutants, the levels of full-length LRRK2 in the kidney (Fig. 5A and E) and brain (Supplementary Material, Fig. S9A) (less in the lung or spleen) were dramatically reduced, while t1 in kidney remained unchanged (Fig. 5E). The spleen contained nearly similar levels of full-length LRRK2 (Fig. 5A) and pull-down experiments using LRRK2-inhibitor coated beads on kidney or brain samples confirmed that active-site ligand binding was retained in the D1994S KD mutant (data not shown). This suggests that improper folding and/or conformational instability of the LRRK2-D1994S full-length protein is an unlikely explanation for its decreased levels in the kidney. The lack of higher levels of KD protein in the insoluble fraction of the homogenized kidney further suggests that this mutant does not have a greatly increased propensity to aggregate (Supplementary Material, Fig. S9B). This view is further supported by our finding that pharmacological inhibition of LRRK2 using a low molecular weight adenosine triphosphate (ATP)-competitive kinase inhibitor (Supplementary Material, Table S2) reduced the level of full-length LRRK2 in the kidney of both WT (Fig. 5F and Supplementary Material, Fig. S10A, a second independent study in WT animals) and, slightly less, also in KI mouse kidney (Supplementary Material, Fig. S10B).

These findings demonstrate the existence of a truncated form of LRRK2 that is present mainly in the kidney. Further, they illustrate that LRRK2 kinase function is needed for the homeostasis of the full-length LRRK2 protein in the kidney.

No overt neuropathology and normal locomotor responses to dopamine agonists/antagonists in KO and KI mice

Unlike the histopathological changes in the kidney and lung, histo- and immunohistochemical evaluation of LRRK2 mutant brain tissue failed to reveal LRRK2-dependent qualitative or quantitative changes. We probed markers for DA neurons [tyrosine hydroxylase (TH), dopamine transporter (DAT)], striatal GABAergic projection neurons [dopamine- and cAMP-regulated neuronal phosphoprotein (DARPP-32)], neurofilament (SMI), α-synuclein (αSN), astrocytes [glial fibrillary acidic protein (GFAP)] and microglia [ionized calcium binding adaptor molecule 1 (Iba1)] and all showed distribution patterns and staining intensities similar to WT littermates (Supplementary Material, Fig. S11; data not shown). Striatal dopamine levels and its metabolites dihydroxyphenyl-acetic acid and homovanillic acid were also unchanged in KO and KI when compared with WT mice (data not shown). Also functional changes in the nigrostriatal system were not detected when probing locomotor responses of KO (Supplementary Material, Figs S12 and S13) and KI (Supplementary Material, Fig. S12) to dopamine D1 and D2 receptor agonists and antagonists (see figures for details). LRRK2 mutations therefore do not result in obvious structural or selected drug-evoked behavioral changes in the nigrostriatal pathway.

DISCUSSION

Here we described several novel aspects of peripheral LRRK2 biology that emerged by studying LRRK2 function in three

different LRRK2 mutant mouse lines. These findings bear on ongoing attempts in various laboratories, to develop LRRK2 selective kinase inhibitors as therapeutics for PD.

LRRK2 plays a role in mouse kidney and lung homeostasis

Our histopathological findings in KO mice reveal an important physiological role of LRRK2 in the mouse kidney and confirm initial observations made in a different line of LRRK2 KO mice (18); LRRK2 deletion leads to kidney darkening and lipofuscin accumulation. Here we demonstrate that these changes manifest already at the age of 5 months, much earlier than reported previously at 20 months of age when both kidney size and weight were found to be reduced (18). In contrast, we found a male gender-specific increase in KO kidney weight starting at the age of 5 months. Note we also observed increased genotype-independent kidney weight in males. Hence, it is important to consider the gender in the analysis. Irrespective, discrepancies between our findings and the previous study may be due to differences in strain background of the mutant mice (ours BALB/c and C57BL/6 versus B6:129 in the previous study). Kidney hypertrophy in KO males might be the result of an increase in protein translation, for example, in response to renal injury as the mice age (32) and/or a decrease in protein degradation (33). In fact, our data suggest that both processes might play a role. We found significantly increased levels of phosphorylated 4E-BP1 reminiscent of reduced 4E-BP1-mediated suppression of protein translational initiation. In addition, we noted an age-dependent accumulation of lipofuscin suggesting impaired proteolysis.

Our findings suggest that the complete absence of the LRRK2 protein or expression of a KD, but not its enhanced (G2019S) kinase variant as has been reported (34), increases 4E-BP1 phosphorylation levels in the kidney, thereby likely regulate protein translation in a LRRK2-dependent fashion (34,35). Higher 4E-BP1 phosphorylation could also be the result of stress-induced protein kinases (13) that might have been activated in KO and KD kidneys. It remains puzzling, however, why kidneys enlarge only in KO males but not in females. In any case, we did not observe kidney abnormalities in heterozygous LRRK2 KO mice that express ~50% less LRRK2 protein when compared with WT mice. Therefore, it appears that the kidney changes occur only after complete loss or a substantial decrease in LRRK2 protein levels as it is the case in the KD kidney (see below).

As early as 6 weeks after birth, a time point that precedes the darkening of the kidneys and the deposition of lipofuscin, we observed abnormal microvacuolization in KO kidney proximal tubule cells, a phenomenon that has not yet been described. Likewise, in KO lungs, type II pneumocytes developed microvacuoles at age 6 weeks. These new findings suggest that LRRK2 plays an important role in both the mouse kidney and lung. Ultrastructural (EM) characterization of adult KO organs clearly showed that the microvacuoles represent secondary lysosomes in renal proximal tubules and lamellar bodies in lung alveolar type II cells. Lamellar bodies are lysosome-related organelles referred to as secretory lysosomes (23). They store and secrete proteins and surfactant phospholipids (organized into tightly packed, bilayer membranes) which reduce surface tension in the alveoli and prevent alveolar collapse during expiration. Further, they contain characteristic lysosomal enzymes (acid phosphatases and cathepsins) and membrane proteins (CD63 and LAMP1) (36–38). Perhaps interesting, we had noted that KO mice manifested breathing difficulties under deep isoflurane anesthesia when we implanted the telemetric devices. How the observed abnormalities in lamellar bodies influence surfactant and lung function needs to be addressed in future studies. In any case, the increased numbers of microvacuoles in both renal proximal tubules and lung alveolar type II cells of KO mice seem to reflect very similar LRRK2-dependent and/or compensatory endosomal–lysosomal pathway changes in both tissues. In the brain, we did not observe similar changes and LRRK2 function in this organ still remains to be elucidated.

LRRK2 protein scaffold versus kinase-domain function

KO mice completely lack the LRRK2 protein. Therefore, phenotypic changes observed in these mutant mice cannot be assigned to the protein's role in scaffolding versus roles exerted by its kinase and/or GTPase domain. To this end, we generated KD mutant mice which developed early-onset (6 weeks after birth) microvacuolation in kidney like KO mice but failed to show a KO-like phenotype in the lung. Most striking were the notably reduced levels of full-length LRRK2 protein levels in the KD kidney (see below for discussion). These levels were even substantially lower than those in the heterozygous KO kidney. In the lung, full-length LRRK2 protein levels were slightly reduced but by far not as marked as in the kidney. These findings imply that the loss of LRRK2 kinase function in the kidney results in a significant reduction in full-length LRRK2 protein levels. Hence, it is difficult to assign a loss-of-function-related phenotype in the KD mutants to the kinase domain. Irrespective, our findings demonstrate that LRRK2 kinase inactivation triggers changes in the kidney that may or may not be desirable.

Interestingly, although similar changes in the kidney occurred in KD and KO mice, only KO mice showed changes in blood pressure. Therefore, it seems highly unlikely that these two changes are causally linked. This is further supported by our findings that also the G2019S KI mutant mice had an increase in diastolic pressure, while these animals showed none of the histopathological kidney changes observed in KO and KD mice. Note, PD patients, including LRRK2 patients, can manifest neurocirculatory abnormalities, including disturbed baroreflexes and/or supine hypertension (39).

So far, none of the histopathological changes observed in the periphery has shown counterparts in the brain and also drug-evoked behavioral responses designed to pick-up potential LRRK2-dependent changes in the nigro-striatal pathway have also largely not met with success. Further studies are needed to elucidate the role of LRRK2 in the nigro-striatal system.

Cell autonomous or non-autonomous role for LRRK2 in altered lysosome homeostasis

We demonstrated an abnormal increase in both number and size of secondary lysosomes in proximal tubule cells of KO and KD kidneys, suggesting a specific role of LRRK2 in

lysosome homeostasis in these specialized cells. This view seems supported also by the finding that lipofuscin accumulates. Lipofuscin consists largely of highly oxidized and cross-linked proteins and lipids that are no longer properly degraded by lysosomes or the proteasomal system. Intracellular accumulation of lipofuscin is a feature of postmitotic aging (40). In adult mouse kidney, LRRK2 mRNA is highly expressed in podocytes and lower in the proximal tubule (41). This could suggest that the abnormal increase in the number of secondary lysosomes in proximal tubule cells is the result of a cell-autonomous LRRK2 defect. Alternatively, this phenotype in proximal tubule cells is a compensatory change in the kidney that might occur secondary to LRRK2-dependent physiological changes elsewhere in the kidney, podocytes being one suspect. We did notice proteinuria in old but not young KO mice that could point to defects in lysosomal function. In the kidney, proteins are filtered in the glomeruli and reabsorbed in the proximal tubule through receptor-mediated endocytosis before being transferred to lysosomes for proteolytic degradation (42). Proteinuria occurs if either glomerular filtration (glomerular proteinuria) or tubular reabsorption of proteins is impaired (tubular proteinuria). The histological changes we observed in proximal tubule cells of KO kidneys and the absence of overt genotype-related changes in glomeruli seem to favor the hypothesis that the proteinuria we observed in old KO mice is due to reduced tubular rather than glomerular function. However, further analyses need to unequivocally discriminate between these possibilities.

The LRRK2 protein has been suggested to localize to the endosomal–lysosomal compartment and pathogenic LRRK2 mutations have been proposed to perturb endosomal–lysosomal trafficking (27,28,43–46). Lysosomal dysfunctions in PD seem frequent. This is exemplified by defective lysosomal glucocerebrosidase function in Gaucher patients where PD risk is highly increased (47,48).

LRRK2 has also been implicated in autophagy (18,27–29). But we did not find alterations in the autophagy marker LC3I/II indicative of either an increase or decrease in autophagy despite an accumulation of a second autophagy marker p62 (49) presumably in secondary lysosomes. p62 is sequestered to autophagosomes and then degraded after fusion with lysosomes (49). Taken together, the data indicate that lysosomal homeostasis is perturbed rather than autophagy itself. Nevertheless, we observed LRRK2 kinase-dependent changes in the kidney mTOR pathway, which is important in controlling autophagy (30). While in the KD kidney TSC2 and mTOR protein levels were decreased, they were increased in KI kidney and, interestingly, also in the KO kidney. The mTOR pathway changes seemed to be organ specific as no change could be observed in the spleen. In addition, they are presumably also independent of kidney pathology as the KD mice, despite similar pathological changes as in KO mice, displayed the opposite effect compared with KO and KI mice, the latter showing no signs of pathology. The observed prominent lower molecular weight protein of mTOR in the kidney may again be pathology independent and is likely to be mTORβ (50), a truncated kinase-active form of mTOR, that perhaps is still capable of phosphorylating 4E-BP1. Truncated forms could be detected for TSC2 and Akt; however, little is known about these forms, opening up speculations of LRRK2 kinase activity involvement in modulating protease activity. Whether the biochemical mTOR-pathway alterations seen in KI and KO mice are causally linked to the directionally similar changes in blood pressure in these mutants remains to be established (51).

Intact LRRK2 kinase function is essential for homeostasis of LRRK2 protein

The levels of the LRRK2 full-length protein were reduced markedly in the KD kidney, whereas other organs showed some (brain > lung) or almost no such effect (spleen). Pharmacological inhibition of LRRK2 kinase in WT and KI mice also reduced LRRK2 full-length protein levels in the kidney. Therefore, a kidney-specific destabilization of the LRRK2-D1994S KD mutant resulting in decreased full-length protein levels seems an unlikely explanation for its decreased levels in the kidney. Rather, these findings demonstrate that the LRRK2 kinase function is essential for maintaining normal LRRK2 full-length steady-state protein levels. Something similar could not be observed *in vitro* in different cell lines overexpressing LRRK2 mutants and treatment with kinase inhibitors (data not shown). Interestingly, a similar mechanism regulating Rip2 levels has been proposed (52). Rip2 has a kinase domain that is closely related to the kinase domain in LRRK2 (53). Although the underlying molecular mechanism remains speculative, it is known that pharmacological inhibition of LRRK2 kinase results in dephosphorylation of its Ser910/Ser935 residues [probably via inhibition of a protein kinase, e.g. PKA that can phosphorylate Ser935 (54) or activation of a protein phosphatase], disruption of 14-3-3 protein binding and altered localization of LRRK2 in the cytoplasm (55,56). However, it was not reported whether kinase inhibitors also change LRRK2 protein levels and future experiments should elucidate the precise molecular mechanism responsible for kinase inhibitor-mediated destabilization of the full-length WT and mutant protein.

We speculate that a decrease in LRRK2 levels, as shown in the KD mutant and following pharmacological inhibition, may also bear on the PD-relevant pathomechanism caused by certain LRRK2 mutants, such as I2020T. This pathogenic familial PD LRRK2 mutation (57) affects an amino acid next to glycine 2019, and was shown to decrease LRRK2 autophosphorylation, the phosphorylation of its putative substrates moesin and myelin basic protein (58) and the artificial substrate LRRKtide (59). Conflicting data aside on whether the I2020T mutation affects kinase activity *per se* (60), it was shown that the LRRK2 I2020T protein is more susceptible to post-translational degradation when compared with WT or the G2019S mutant (60). Nonetheless, the value of these findings will become apparent if they translate, for example, to human I2020T patient fibroblasts. Following the same line of thought, it is more difficult to explain the pathogenic effects of the G2019S mutation which enhances kinase activity and did not show any destabilization effects on the protein in the kidney of mutant mice. We can only speculate. But the finding that physiological changes in blood pressure show the same direction in KO and G2019S mutants could suggest that the net output of LRRK2 signaling by the G2019S mutant and the full KO might be similar.

In summary, we show that expression of KD LRRK2 leads to early-onset histopathological abnormalities in the kidney (microvacuoles, lipofuscin deposits) indistinguishable from those observed in mice lacking LRRK2. KO but not KD mice develop a similar pathology in lung, suggesting that a LRRK2 scaffold and/or GTPase rather than its kinase function is causally linked to abnormalities in the lung. Diastolic blood pressure changes in both KI and KO but not KD mice seem to suggest that these physiological changes are LRRK2 kinase function independent and the fact that they occur in G2019S mutants demonstrates that they are independent of kidney histopathological changes seen in KO and KD mutants. Finally, LRRK2 kinase function determines the stability of the full-length LRRK2 protein and kinase inhibition lowers LRRK2 protein levels. Appreciating the molecular complexity of LRRK2 signaling and phenotypic changes calls for a cautious evaluation of LRRK2-directed therapeutics.

MATERIALS AND METHODS

Statement on animal health

All experiments were carried out in accordance with the authorization guidelines of the Swiss federal and cantonal veterinary offices for the care and use of laboratory animals. Studies described in this report were approved by the Swiss cantonal veterinary office and performed according to Novartis animal license numbers 2063, 2382 and 95.

Generation of LRRK2 gene-modified mice

Cloning of the LRRK2-G2019S targeting vector. *LRRK2* genomic sequences containing exon 41 were amplified from Balb/c mouse genomic DNA and subcloned. Site-directed mutagenesis was performed to modify codon GGG (Gly) to TCG (Ser), resulting in the desired G2019S mutation in exon 41. A loxP element was inserted into a *Bgl*I restriction site 5′ of exon 41. Modified genomic sequences were excised by *Hin*dIII and subcloned into the *Hin*dIII restriction site of pRAY2 (Accession No. U63120). *LRRK2* genomic sequences downstream of exon 41 were amplified as described above and subcloned using *Cla*I/*Not*I into pRAY2 containing the cloned modified exon, resulting in the *LRRK2* target plasmid.

Cloning of the LRRK2-D1994S targeting vector. *LRRK2* genomic sequences flanking exon 41 were amplified from Balb/c mouse genomic DNA and subcloned. Overlapping polymerase chain reaction (PCR) was performed to modify codon GAC (Asp) to TCC (Ser), resulting in the desired D1994S mutation in exon 41. Modified genomic sequences were subcloned into the *Hpa*I/*Xho*I-digested vector pRAY2-LRRK2 5′ arm. *LRRK2* genomic sequences downstream of exon 41 were amplified as described above and subcloned using *Cla*I/*Not*I into pRAY2 containing the cloned modified exon, resulting in the plasmid *LRRK2*-D1994S target. Subcloned sequences were compared with sequences available from the Ensembl database (Ensembl Gene ID ENSMUSG00000036273).

Transfection of mouse embryonic stem cells. Embryonic stem (ES) cells were cultured in 6 cm dishes containing primary X-ray-inactivated embryonic fibroblast cells from DR4 mice (TgN(DR4)1Jae (61). ES cells were transfected by electroporation of 20 μg of *Not*I-digested pLRRK2 target plasmid. Transfected ES cells were selected for neomycin resistance with 0.2 mg/ml geneticin (G418, Invitrogen #10131-019). Ten days after transfection, G418-resistant ES cell clones were isolated and analyzed by PCR (nested PCR: first PCR: sense primer: Neo-4: TCC TCG TGC TTT ACG GTA; antisense primer: LRRK2-rev1: CCC GTC AGT AAG TGA GCT; second PCR: sense primer: Neo-5: CTA TCG CCT TCT TGA CGA A; antisense primer: LRRK2-rev2: CTT TGA CCT TGG GAT GAA) for homologous recombination. An additional PCR was performed to control for the presence of the *lox*P element 5′ of *LRRK2* exon 41 (sense primer: LRRK2-geno.for: GTG TTA AAG CTC CAG TTG CCT; antisense primer: LRRK2-geno.rev: GCC AGA GAG TAC ACA GGA GGT).

To eliminate the flp recombinase recognition site (FRT)-flanked neomycin cassette in ES cells, cells were co-transfected with the plasmids pEGFP-N1 (Accession No. U55762) and pCAG-FLP at a ratio of 1:4 using Lipofectamine^{TM} 2000 (Invitrogen #11668-027) as transfection reagent. Two days after transfection, enhanced green fluorescent protein-expressing ES cells were collected by fluorescence-activated cell sorting (FACS) (FACSCalibur, Becton Dickinson) and cultured for a further 6 days in normal media. Forty-eight single clone cells were selected and split onto two plates. Cell culture was performed on a 96-well plate with feeder (0.5×10^6 inactivated feeder cells/96-well plate) in the ES medium with or without G418 (0.2 mg/ml G418). PCR to control for Flp-mediated FRT recombination and excision of the neomycin cassette were performed (sense primer: LRRK2-geno.for: GTG TTA AAG CTC CAG TTG CCT; antisense primer: FRT(-neo)rev: TTT CGA ACC CGG GGA AGT TC).

Southern blot analysis. Homologous recombination of the targeting plasmid into the *LRRK2* locus was verified by southern hybridization. For this purpose, genomic DNA from ES cell colonies was digested with the restriction enzyme *Eco*RV, blotted and hybridized with a labeled neomycin probe. In brief, 5 μg of genomic DNA were digested with 30 units of the restriction enzyme and separated on a 0.9% agarose gel. After denaturation, the DNA was blotted on a Hybond N+ membrane (Amersham #RPN203B) followed by UV crosslinking. Hybridization with the ^{32}P-labeled DNA probe (Rediprime II Random prime labeling kit, Amersham #RPN1633) was performed in Perfect Plus Hybridization buffer (Sigma #H7033) at 65°C overnight. After washing of the hybridized membrane, image analysis was performed using a phosphoimager.

Blastocyst injection and generation of gene-modified animals. Targeted Balb/c ES cells were injected into C57Bl/6J host blastocysts, which were then transferred into pseudopregnant B6CF1 foster mothers. Chimeric offspring were identified by coat pigmentation [white (Balb/c) on a black (C57Bl/6J) background]. White offspring indicated the germline transmission of the targeted ES cells and were further analyzed for their correct genotype.

We generated LRRK2 KO mice by crossing chimeric LRRK2 G2019S KI males with either BALB/c or C57Bl/6J Cre-deleter females (B6-TgN(CMV-Cre)#Cgn (62) that express the Cre recombinase in the fertilized oocyte, resulting in deletion of the floxed fragment in all cells of the organism (KO). Offsprings of the crossing were analyzed by PCR to identify mice in which Cre recombination has taken place. Cre recombination should take place in offspring containing both the targeted LRRK2 allele as well as the gene for Cre recombinase. This event should result in a PCR product of 150 bp instead of 816 bp from the non-recombined allele (sense primer: LRRK2-geno.for: GTG TTA AAG CTC CAG TTG CCT; antisense primer: FRT(-neo)rev: TTT CGA ACC CGG GGA AGT TC).

Mice were kept either in BALB/c background or were backcrossed into C57Bl/6J. For backcrossing of LRRK2 KO and KI lines into C57Bl/6J we applied speed congenics. For the experiments, we used mice that were backcrossed either at least six generations or at least two generations (LRRK2 KD and aged LRRK2 KI) into C57Bl/6J.

Non-transgenic control mice were either littermates (from a heterozygous breeding) or from a WT breeding of the respective line from the same generation to reduce animal numbers.

Genotyping

Gene-modified mice were selected by standard Taqman PCR analysis of tail DNA with primers and fluorescently labeled probes: KD: LRRK2-2lox.for TA (5′-CGA AAA CAG CAA CAA CGA CAA C-3′), LRRK2-2lox.rev TA (5′-ATA GGA ACT TCT TGG CTG GAC-3′), LRRK2.KD-probe (5′-FAM-TCC GAG CCA AAA ACT CTC GAG GAA TT-TAMRA-3′); KI: LRRK2-2lox.for TA (5′-CGA AAA CAG CAA CAA CGA CAA C-3′), LRRK2-2lox.rev TA (5′-ATA GGA ACT TCT TGG CTG GAC-3′), LRRK2.2lox-probe (5′-FAM-TCC GAG CCA AAA ACT AAG CTT CTC GA-TAMRA-3′); KO: LRRK2.for (5′-TGT ATC CCA ATG CTG CCA TC-3′), LRRK2.rev (5′-CTA TAT CTC CTA GAC CCA CAC-3′), LRRK2.Ex41.probe (5′-YYE-TGG GAA TAA AGA CAT CAG AGG GCA C-TAMRA-3′). As endogenous control PCR: αSN-5′ (5′-GCT GGA AAG ACA AAA GAG GG-3′), αSN-3′ (5′-ATT CTC TCA CCT CCA CAC AG-3′), αSN-probe (5′-FAM or YYE-TGG CTG GTG TGT GGT GTC TGA TT-TAMRA-3′). Rotorgene 3000 was used for PCR (at 95°C for 10 min, 40 cycles at 95°C for 15 s and at 60°C for 1 min).

Immunoblot analysis

For near-infrared Li-cor western blot analysis, kidneys and brains were homogenized in homogenization buffer (10v/w) (additional phosphatase and protease inhibitors: 50 mM Tris–HCl, pH 7.4; 150 mM NaCl; 1.5 mM $MgCl_2$; 5% glycerol; 1 mM Na_3VO_4; 25 mM NaF; 1 mM dithiothreitol (DTT); 0.8% NP-40 (add NaF, DTT and NP-40 just before use), complete ethylenediaminetetraacetic acid (EDTA)-free protease inhibitors (Roche), 0.5 mM PMSF (Sigma), 5 μg/ml Pepstatin A (Sigma), 5 μg/ml Leupeptin (Sigma), 1:1000 Okadaic acid 100 ng/μl in ethanol (Biomol), 1:1000 Calyculin A 100 ng/μl in ethanol (Biosource), 1:100 Pierce phosphatase inhibitor cocktail ×100 with Precellys24 (Bertin Technologies, rotation speed 5000 rpm, number of cycles: brain—2 × 30 s, pause: 10 s; kidney—2 × 50 s, Pause: 10 s), then incubated for 30 min on ice and subsequently centrifuged at 13K rpm at 4°C for 10 min.

Homogenization buffer containing only standard phosphatase and protease inhibitors: 10 v/w; 0.25 M sucrose, 20 mM Tris 20 mM pH 7.4, 1 mM EDTA, 1 mM EGTA, protease inhibitor cocktail (Roche).

Homogenization buffer containing additional phosphatase and but only standard protease inhibitors: 10 v/w; 0.25 M sucrose, 20 mM Tris 20 mM pH 7.4, 1 mM EDTA, 1 mM EGTA, 1:1000 Okadaic acid 100 ng/μl in ethanol, 1:1000 Calyculin A 100 ng/μl in ethanol, 1:100 Pierce phosphatase inhibitor cocktail, protease inhibitor cocktail (Roche).

Supernatant and pellet (resuspended in homogenization buffer in the same volume used for homogenization) was used and protein concentration was determined from the supernatant by Bradford (Bio-Rad). Thirty microgram protein of the supernatant was loaded (LDS Sample Buffer, Sample Reducing Agent, Invitrogen, heated for 10 min at 95°C) on NuPAGE 4–12% Bis–tris gel 1.0 mM (Invitrogen) and ran at 180 V for 40–50 min with NuPAGE MES SDS Running Buffer (Invitrogen) or NuPAGE 3–8% Tris-Acetate gel 1.0 mM ran at 150 V for 60 min with Tris-Acetate SDS running buffer (Invitrogen). Gels were blotted by semi wet transfer (Invitrogen × Cell II Blot Module) with NuPAGE Transfer Buffer, 10% (for one gel) or 20% methanol (for two gels) on polyvinylidene difluoride transfer membrane (Immobilon-P, Invitrogen) at constant 30 V for 1 h. For Li-cor Odyssey detection, membrane was blocked for 1 h at room temperature in Odyssey Blocking Buffer (Odyssey, 1:1 diluted with phosphate buffered saline (PBS)) and then incubated with primary antibody in Odyssey Blocking Buffer (diluted 1:1 with PBS, containing 0.1% or 0.05% Tween 20) overnight at 4°C. Primary antibodies used: mouse anti-β-actin (Sigma, 1:50000); anti-LRRK2 MJJF2 c41 (Michael J. Fox Foundation/Epitomics, 1:2500); mouse anti-α-synuclein (BD Transduction, 1:5000); all subsequent antibodies were from Cell Signaling (rabbit polyclonal, exceptions indicated) and used at 1:1000: anti-S6 (rabbit monoclonal), anti-P-S6(Ser235/236), anti-4E-BP1, anti-P-4E-BP1(Thr37/46), anti-Akt, anti-P-Akt(S473), anti-TSC2, anti-LC3B and anti-mTOR. Membranes were washed four times for 5 min at room temperature in PBS containing 0.1% or 0.05% Tween 20 and then incubated for 45 min (light protected) with second antibodies [Alexa Fluor 680, F(ab′)2 fragment of goat anti-mouse (Invitrogen); IRDye 800CW anti-rabbit IgG (Li-cor); both 1:5000] in Odyssey Blocking Buffer (diluted 1:1 in PBS, containing 0.1% or 0.05% Tween20). Membranes were again washed four times for 5 min at room temperature in PBS containing 0.1% or 0.05 Tween 20, then washed two times for 5 min at room temperature in PBS only and finally scanned on the Odyssey Li-cor System.

Kinase assay

The Bac-to-Bac Baculovirus Expression System (Invitrogen) was used (according to the protocol of the manufacturer) to express N-terminal HIS-GST-tagged (6×Histidine- and

Glutathion-S-Transferase-tag) human LRRK2 constructs. The LRRK2 constructs consisted of a part of LRRK2 (amino acids 1675–2527) which produced stable and active LRRK2 protein (HIS-GST-hLRRK2 1675-2527 G2019S and HIS-GST-hLRRK2 1675-2527 D1994S). Cells were harvested, centrifuged at 3000 rpm for 7 min and HIS-GST-hLRRK2 1675-2527 G2019S and D1994S were purified by GST SpinTrap columns (GE Healthcare Life Sciences). Briefly, the cell pellet was lysed in lysis buffer (50 mM Tis–HCl, 150 mM NaCl, 2 mM DTT, 0.02% Tween 20, 0.5 mM EDTA, 20% glycerol, 1X complete (protease inhibitors, Roche). Centrifugation, sonication and purification were performed according to the protocol of the manufacturer (GE Healthcare Life Sciences). Lysate were applied to the GST SpinTrap column, washed once with PBS, then three times with washing buffer (20 mM Tris–HCl, 2 mM DTT, 0.1 mg/ml bovine serum albumin (BSA), 0.5 mM EDTA, 20% glycerol, 1 mM Na_3VO_4, 5 mM β-glycerophosphate) and eluted with elution buffer (50 mM Tris–HCl, 0.1 mg/ml BSA, 20% glycerol, 5 mM β-glycerophosphate, 10 mM GSH (reduced glutathione, GE Healthcare Life Sciences). The kinase reaction was performed by diluting the components to 3-fold final concentration in 1× kinase buffer (50 mM Hepes, 1 mM DTT, 0.6 mM EGTA, 10 mM $MgCl_2$, 3 mM $MnCl_2$): ATP to 750 mM (10 mM ATP stock; Biolabs), GST-4xLRRKTide long [as a 4× repeat fused to GST, (58)] to 6 mM, while GST SpinTrap elution fraction #1 was not diluted. The final reaction volume was 15 μl: 5 μl 3x ATP, 5 μl 3x GST-LRRKtide and 5 μl GST-hLRRK2 1675-2527 constructs. Reaction was incubated for 30 min at room temperature, stopped by adding 5 μl 4xLDS sample buffer (Invitrogen, with 200 mM DTT) and heating to 90°C for 10 min, analyzed on western blot (4–12% Tris-Acetate gels and semi-dry blotting, Invitrogen) using anti-LRRK2 CK (homemade, directed against the c-terminus of the kinase domain of LRRK2; rabbit, 1:500) and anti-phospho-ezrin (rabbit, Cell Signaling Technology, 1:1000) antibodies and visualized with Li-Cor Odyssey.

Histopathological analysis

Following necropsy, organs were fixed in 4% neutral phosphate-buffered formalin for 1 day, then transferred to PBS, trimmed, embedded in paraffin wax, sectioned and stained with hematoxylin and eosin (H&E) or left unstained for autofluorescence analysis. The tissue slices were evaluated and reviewed by pathologists.

Immunohistochemistry

Antibodies/dilutions used for immunohistochemistry and immunofluorescence staining:

primary antibodies: polyclonal rabbit anti-LAMP1 (Abcam ab24210); monoclonal rat anti-LAMP2 (SouthernBiotech; 1:250); polyclonal rabbit anti-MUC1 (Mucin-1) (Abcam ab15481); polyclonal rabbit anti-GFAP (DAKO #Z0334; 1:5000); polyclonal rabbit anti-Iba1 (WAKO chemicals, #019-19471; 1:500); polyclonal rabbit anti-TH (Novus Biologicals NB300-109; 1:500); monoclonal rat anti-DAT (Chemicon MAB369; 1:200); monoclonal rabbit anti-DARPP-32 (Cell Signalling # 2306; 1:500); polyclonal rabbit anti-α-synuclein (Chemicon AB 5038; 1:1000); monoclonal mouse anti-α-synuclein (Abcam 4D6; 1:1000); polyclonal guinea pig anti-p62 (C-terminus) (Progen, 1:100); monoclonal mouse anti-neurofilament (Covance SMI310R; 1:1000). Secondary antibodies: biotinylated goat anti-guinea pig (Vectorlabs, 1:200); biotinylated goat anti-mouse (Jackson ImmunoResearch; 1:1000); biotinylated goat anti-rat (Jackson ImmunoResearch; 1:1000); biotinylated goat anti-rabbit (Jackson ImmunoResearch; 1:1000); Alexa488-labeled goat anti-rat (Invitrogen, 1:500); Alexa488-labeled goat anti-rabbit (Invitrogen; 1:500).

Automated immunohistochemistry. Mice were transcardially perfused first with PBS and then with 4% paraformaldehyde in PBS. Brains and kidneys were prepared, postfixed for another 2 days at 4°C with 4% paraformaldehyde in PBS and embedded in paraffin according to standard procedures. Four micrometer para-sagittal paraffin sections were mounted on SuperFrost Plus slides and automatically immunostained using the Discovery XT technology (Ventana/Roche diagnostics). Briefly, sections were deparaffinized, rehydrated, subjected to antigen retrieval by heating with CC1 cell conditioning buffer (Ventana/Roche Diagnostics), incubated for 60 min at room temperature with primary antibody diluted in antibody diluent (Ventana/Roche Diagnostics), incubated with the respective biotinylated secondary antibody diluted in Ventana antibody dilution, reacted with DABMab kit (Ventana/Roche Diagnistics) and counterstained with blueing reagent (Ventana/Roche Diagnostics). Digital slides were generated with MIRAX (Zeiss) scanner technology.

Manual immunohistochemistry and immunfluorescence staining of DARPP-32, TH and DAT for quantitative image analysis. Paraffin sections were dewaxed, rehydrated, subjected to antigen retrieval by microwaving the slides for 10 min at 98°C in 0.1 M citrate buffer pH 6.0, incubated for 1 h at room temperature in PBS containing 2% goat serum, reacted over night at 4°C with primary antibody diluted in PBS/2% goat serum, stained with the appropriate Alexa488- or Biotin-labeled secondary goat antibody diluted in PBS. For the biotin-labeled secondary antibody ABC reagent (Vectorlabs) for 1 h at room temperature was applied with subsequent washes in PBS, developed with DAB stain, desalted in 0.01 M Tris (pH 7.8) and mounted with Eu-kitt. Immunofluorescence-stained slides were mounted with ProLong antifade containing 4′,6-diamidino-2-phenylindole (DAPI) (Invitrogen). Immunofluorescence in the striatum was imaged, at consistent exposure time for the respective marker, with an Olympus BX51 microscope equipped with appropriate fluorescence filters and colorview III digital camera. Fluorescence intensity in the striatum was analyzed with CellF image analysis software (Soft Imaging Systems/Olympus). Each six sagittal sections were analyzed per animal.

Electron microscopy

Kidneys and lungs were fixed with 3% glutaraldehyde in 0.1 M cacodylate buffer, pH 7.4, for about 1 h at 4°C and 1% OsO_4 in 0.1 M cacodylate buffer, pH 7.4, for 1 h at 4°C. After post-

fixation, the tissues were dehydrated in graded acetone solutions, and embedded in Epon. For microscopic evaluation, semi-thin sections were prepared from tissue blocks, stained with toluidine blue and examined with a Zeiss light microscope. Based on these light microscopic investigations, ultrathin sections from selected tissue blocks were counterstained with uranyl acetate and lead citrate and examined with a Philips CM 10 transmission electron microscope.

Urinalysis

Urine samples were collected into plain tubes. Total protein and creatinine were determined, using a Cobas 6000® analyzer. Urine total protein concentration was analyzed with the benzethonium chloride assay with a γ-globulin recovery rate which is 30% less than that of albumin.

Telemetric blood pressure and heart rate measurements

The radio-telemetry system (Data Sciences Int.) used in this study is composed of four basic components: an implantable transmitter (AM unit, model TLM-PAC10, volume: 1.1 cc, weight: 1.4 g) which continuously senses and transmits information from within the animal, one receiver located under the home cage, a matrix interface for coordination of signals and a computer-based data acquisition system for collection, analysis and storage of data. The body of the transmitter was implanted s.c. in aseptic conditions into the flank of the animal under isoflurane anesthesia. The sensing catheter was inserted into the left femoral artery. The total operation time for the implantation of the telemetry transmitter was about 40 min. Postoperative analgesia was provided using Buprenorphin (Temgesic®) injection of 0.05 mg/kg s.c. twice, immediately after surgery and 8–12 h later. Following surgery, the unconscious animal is placed on soft material in a clean cage with water ad libitum. The animals were allowed a period of 2–3 weeks to recover from surgery before starting acquisition of any physiological data. Mean, systolic and diastolic blood pressure and heart rate were recorded continuously in all animals over 24 h up to 8 days, and analyzed in 1 min cyclic runs for 10 s with a 500 Hz sampling rate.

Motility cages

Locomotor activity was measured with the TSE system (process control type 302013-CD, software: Motilitätsmess-system 4.2) in motility cages (Makrolon Typ III with a lid and without embedding). Cages were changed after each animal. After the habituation phase (30–60 min), animals were taken out of the cage, administered the drug and then placed back into the cage and further monitored for motility (30–60 min). The dopamine-receptor antagonist/agonists SCH23390, haloperidol, quinpirole and SKF38393 (all from Sigma) were administered s.c. in a physiological NaCl solution. D-amphetamine hemisulfate (Sigma) and cocaine-HCl (Sigma) were administered i.p. (10 ml/kg) in a physiological NaCl solution.

Animal maintenance and LRRK2 kinase inhibitor drug administration

The animals were housed in a temperature-controlled room that was maintained on a 12 h light/dark cycle. Food and water were available ad libitum. Mice were administered orally with 30 mg/kg LRRK2 kinase inhibitor compound (dissolved in 0.5% methylcellulose with 0.5% Tween 80, administration volume 10 ml/kg) twice daily (morning/afternoon) for 5 days and were killed 2 h after last dosing. Novartis is willing to provide said LRRK2 kinase inhibitor under a material transfer agreement for academic research and non-commercial purposes.

SUPPLEMENTARY MATERIAL

Supplementary Material is available at *HMG* online.

ACKNOWLEDGMENTS

We thank Graeme Bilbe for critically reading the manuscript and Janina Hanne, Jean-Jacques Feldtrauer, Etienne Regulier, Petranka Krumova, Maxime Magnier, Daniela Stauffer, Yves Auberson, Mario Centeleghe, Nella Vidotto and Mario Bernhard for their support.

Conflict of Interest statement. None declared.

FUNDING

The work was funded by the Novartis Pharma AG. The company had a role in this study due to employment of one or more authors of this study. Funding to pay the Open Access publication charges for this article was provided by Novartis Pharma AG.

REFERENCES

1. Esposito, E., Di Matteo, V. and Di Giovanni, G. (2007) Death in the substantia nigra: a motor tragedy. *Expert Rev. Neurother.*, **7**, 677–697.
2. Healy, D.G., Falchi, M., O'Sullivan, S.S., Bonifati, V., Durr, A., Bressman, S., Brice, A., Aasly, J., Zabetian, C.P., Goldwurm, S. *et al.* (2008) Phenotype, genotype, and worldwide genetic penetrance of LRRK2-associated Parkinson's disease: a case-control study. *Lancet Neurol.*, **7**, 583–590.
3. Zimprich, A., Biskup, S., Leitner, P., Lichtner, P., Farrer, M., Lincoln, S., Kachergus, J., Hulihan, M., Uitti, R.J., Calne, D.B. *et al.* (2004) Mutations in LRRK2 cause autosomal-dominant parkinsonism with pleomorphic pathology. *Neuron*, **44**, 601–607.
4. Paisan-Ruiz, C., Jain, S., Evans, E.W., Gilks, W.P., Simon, J., van der Brug, M., Lopez de Munain, A., Aparicio, S., Gil, A.M., Khan, N. *et al.* (2004) Cloning of the gene containing mutations that cause PARK8-linked Parkinson's disease. *Neuron*, **44**, 595–600.
5. Simon-Sanchez, J., Schulte, C., Bras, J.M., Sharma, M., Gibbs, J.R., Berg, D., Paisan-Ruiz, C., Lichtner, P., Scholz, S.W., Hernandez, D.G. *et al.* (2009) Genome-wide association study reveals genetic risk underlying Parkinson's disease. *Nat. Genet.*, **41**, 1308–1312.
6. Satake, W., Nakabayashi, Y., Mizuta, I., Hirota, Y., Ito, C., Kubo, M., Kawaguchi, T., Tsunoda, T., Watanabe, M., Takeda, A. *et al.* (2009) Genome-wide association study identifies common variants at four loci as genetic risk factors for Parkinson's disease. *Nat. Genet.*, **41**, 1303–1307.
7. International Parkinson Disease Genomics Consortium. (2011) Imputation of sequence variants for identification of genetic risks for Parkinson's disease: a meta-analysis of genome-wide association studies. *Lancet*, **377**, 641–649.

8. Cookson, M.R. (2010) The role of leucine-rich repeat kinase 2 (LRRK2) in Parkinson's disease. *Nat. Rev. Neurosci.*, **11**, 791–797.
9. Barrett, J.C., Hansoul, S., Nicolae, D.L., Cho, J.H., Duerr, R.H., Rioux, J.D., Brant, S.R., Silverberg, M.S., Taylor, K.D., Barmada, M.M. *et al.* (2008) Genome-wide association defines more than 30 distinct susceptibility loci for Crohn's disease. *Nat. Genet.*, **40**, 955–962.
10. Looyenga, B.D., Furge, K.A., Dykema, K.J., Koeman, J., Swiatek, P.J., Giordano, T.J., West, A.B., Resau, J.H., Teh, B.T. and MacKeigan, J.P. (2011) Chromosomal amplification of leucine-rich repeat kinase-2 (LRRK2) is required for oncogenic MET signaling in papillary renal and thyroid carcinomas. *Proc. Natl Acad. Sci. USA*, **108**, 1439–1444.
11. Anand, V.S. and Braithwaite, S.P. (2009) LRRK2 in Parkinson's disease: biochemical functions. *FEBS J.*, **276**, 6428–6435.
12. West, A.B., Moore, D.J., Biskup, S., Bugayenko, A., Smith, W.W., Ross, C.A., Dawson, V.L. and Dawson, T.M. (2005) Parkinson's disease-associated mutations in leucine-rich repeat kinase 2 augment kinase activity. *Proc. Natl Acad. Sci. USA*, **102**, 16842–16847.
13. Kumar, A., Greggio, E., Beilina, A., Kaganovich, A., Chan, D., Taymans, J.M., Wolozin, B. and Cookson, M.R. (2010) The Parkinson's disease associated LRRK2 exhibits weaker in vitro phosphorylation of 4E-BP compared to autophosphorylation. *PLoS ONE*, **5**, e8730.
14. Dusonchet, J., Kochubey, O., Stafa, K., Young, S.M. Jr, Zufferey, R., Moore, D.J., Schneider, B.L. and Aebischer, P. (2011) A rat model of progressive nigral neurodegeneration induced by the Parkinson's disease-associated G2019S mutation in LRRK2. *J. Neurosci.*, **31**, 907–912.
15. Iaccarino, C., Crosio, C., Vitale, C., Sanna, G., Carri, M.T. and Barone, P. (2007) Apoptotic mechanisms in mutant LRRK2-mediated cell death. *Hum. Mol. Genet.*, **16**, 1319–1326.
16. Smith, W.W., Pei, Z., Jiang, H., Dawson, V.L., Dawson, T.M. and Ross, C.A. (2006) Kinase activity of mutant LRRK2 mediates neuronal toxicity. *Nat. Neurosci.*, **9**, 1231–1233.
17. Lee, B.D., Shin, J.H., VanKampen, J., Petrucelli, L., West, A.B., Ko, H.S., Lee, Y.I., Maguire-Zeiss, K.A., Bowers, W.J., Federoff, H.J. *et al.* (2010) Inhibitors of leucine-rich repeat kinase-2 protect against models of Parkinson's disease. *Nat. Med.*, **16**, 998–1000.
18. Tong, Y., Yamaguchi, H., Giaime, E., Boyle, S., Kopan, R., Kelleher, R.J. 3rd and Shen, J. (2010) Loss of leucine-rich repeat kinase 2 causes impairment of protein degradation pathways, accumulation of alpha-synuclein, and apoptotic cell death in aged mice. *Proc. Natl Acad. Sci. USA*, **107**, 9879–9884.
19. Finch, C.E. (1993) Neuron atrophy during aging: programmed or sporadic? *Trends Neurosci.*, **16**, 104–110.
20. Reichel, W. (1968) Lipofuscin pigment accumulation and distribution in five rat organs as a function of age. *J. Gerontol.*, **23**, 145–153.
21. Ochs, M. (2010) The closer we look the more we see? Quantitative microscopic analysis of the pulmonary surfactant system. *Cell. Physiol. Biochem.*, **25**, 27–40.
22. Zhao, C.Z., Fang, X.C., Wang, D., Tang, F.D. and Wang, X.D. (2010) Involvement of type II pneumocytes in the pathogenesis of chronic obstructive pulmonary disease. *Respir. Med.*, **104**, 1391–1395.
23. Weaver, T.E., Na, C.L. and Stahlman, M. (2002) Biogenesis of lamellar bodies, lysosome-related organelles involved in storage and secretion of pulmonary surfactant. *Semin. Cell Dev. Biol.*, **13**, 263–270.
24. Cruz, D.N., Simon, D.B., Nelson-Williams, C., Farhi, A., Finberg, K., Burleson, L., Gill, J.R. and Lifton, R.P. (2001) Mutations in the Na-Cl cotransporter reduce blood pressure in humans. *Hypertension*, **37**, 1458–1464.
25. Wilson, F.H., Disse-Nicodeme, S., Choate, K.A., Ishikawa, K., Nelson-Williams, C., Desitter, I., Gunel, M., Milford, D.V., Lipkin, G.W., Achard, J.M. *et al.* (2001) Human hypertension caused by mutations in WNK kinases. *Science*, **293**, 1107–1112.
26. Lifton, R.P., Gharavi, A.G. and Geller, D.S. (2001) Molecular mechanisms of human hypertension. *Cell*, **104**, 545–556.
27. Alegre-Abarrategui, J., Christian, H., Lufino, M.M., Mutihac, R., Venda, L.L., Ansorge, O. and Wade-Martins, R. (2009) LRRK2 regulates autophagic activity and localizes to specific membrane microdomains in a novel human genomic reporter cellular model. *Hum. Mol. Genet.*, **18**, 4022–4034.
28. Plowey, E.D., Cherra, S.J. 3rd, Liu, Y.J. and Chu, C.T. (2008) Role of autophagy in G2019S-LRRK2-associated neurite shortening in differentiated SH-SY5Y cells. *J. Neurochem.*, **105**, 1048–1056.
29. Xiong, Y., Coombes, C.E., Kilaru, A., Li, X., Gitler, A.D., Bowers, W.J., Dawson, V.L., Dawson, T.M. and Moore, D.J. (2010) GTPase activity plays a key role in the pathobiology of LRRK2. *PLoS Genet.*, **6**, e1000902.
30. Wong, E. and Cuervo, A.M. (2010) Autophagy gone awry in neurodegenerative diseases. *Nat. Neurosci.*, **13**, 805–811.
31. Chen, J.K., Chen, J., Neilson, E.G. and Harris, R.C. (2005) Role of mammalian target of rapamycin signaling in compensatory renal hypertrophy. *J. Am. Soc. Nephrol.*, **16**, 1384–1391.
32. Kasinath, B.S., Feliers, D., Sataranatarajan, K., Ghosh Choudhury, G., Lee, M.J. and Mariappan, M.M. (2009) Regulation of mRNA translation in renal physiology and disease. *Am. J. Physiol. Renal. Physiol.*, **297**, F1153–F1165.
33. Franch, H.A. (2002) Pathways of proteolysis affecting renal cell growth. *Curr. Opin. Nephrol. Hypertens.*, **11**, 445–450.
34. Imai, Y., Gehrke, S., Wang, H.Q., Takahashi, R., Hasegawa, K., Oota, E. and Lu, B. (2008) Phosphorylation of 4E-BP by LRRK2 affects the maintenance of dopaminergic neurons in Drosophila. *EMBO J.*, **27**, 2432–2443.
35. Gehrke, S., Imai, Y., Sokol, N. and Lu, B. (2010) Pathogenic LRRK2 negatively regulates microRNA-mediated translational repression. *Nature*, **466**, 637–641.
36. Huizing, M., Helip-Wooley, A., Westbroek, W., Gunay-Aygun, M. and Gahl, W.A. (2008) Disorders of lysosome-related organelle biogenesis: clinical and molecular genetics. *Annu. Rev. Genomics Hum. Genet.*, **9**, 359–386.
37. Young, B. and Heath, J.W. (2002) *Wheater's Functional Histology: A Text and Colour Atlas*. Elsevier Science.
38. Ghadially, F.N. (1975) *Ultrastructural Pathology of the Cell: A Text and Atlas of Physiological and Pathological Alterations in Cell Fine Structure*. Butterworths, London.
39. Goldstein, D.S., Imrich, R., Peckham, E., Holmes, C., Lopez, G., Crews, C., Hardy, J., Singleton, A. and Hallett, M. (2007) Neurocirculatory and nigrostriatal abnormalities in Parkinson disease from LRRK2 mutation. *Neurology*, **69**, 1580–1584.
40. Jung, T., Bader, N. and Grune, T. (2007) Lipofuscin: formation, distribution, and metabolic consequences. *Ann. N Y Acad. Sci.*, **1119**, 97–111.
41. Zechel, S., Meinhardt, A., Unsicker, K. and von Bohlen Und Halbach, O. (2010) Expression of leucine-rich-repeat-kinase 2 (LRRK2) during embryonic development. *Int. J. Dev. Neurosci.*, **28**, 391–399.
42. Christensen, E.I., Verroust, P.J. and Nielsen, R. (2009) Receptor-mediated endocytosis in renal proximal tubule. *Pflugers Arch.*, **458**, 1039–1048.
43. MacLeod, D., Dowman, J., Hammond, R., Leete, T., Inoue, K. and Abeliovich, A. (2006) The familial Parkinsonism gene LRRK2 regulates neurite process morphology. *Neuron*, **52**, 587–593.
44. Shin, N., Jeong, H., Kwon, J., Heo, H.Y., Kwon, J.J., Yun, H.J., Kim, C.H., Han, B.S., Tong, Y., Shen, J. *et al.* (2008) LRRK2 regulates synaptic vesicle endocytosis. *Exp. Cell Res.*, **314**, 2055–2065.
45. Biskup, S., Moore, D.J., Celsi, F., Higashi, S., West, A.B., Andrabi, S.A., Kurkinen, K., Yu, S.W., Savitt, J.M., Waldvogel, H.J. *et al.* (2006) Localization of LRRK2 to membranous and vesicular structures in mammalian brain. *Ann. Neurol.*, **60**, 557–569.
46. Higashi, S., Moore, D.J., Yamamoto, R., Minegishi, M., Sato, K., Togo, T., Katsuse, O., Uchikado, H., Furukawa, Y., Hino, H. *et al.* (2009) Abnormal localization of leucine-rich repeat kinase 2 to the endosomal-lysosomal compartment in lewy body disease. *J. Neuropathol. Exp. Neurol.*, **68**, 994–1005.
47. Neumann, J., Bras, J., Deas, E., O'Sullivan, S.S., Parkkinen, L., Lachmann, R.H., Li, A., Holton, J., Guerreiro, R., Paudel, R. *et al.* (2009) Glucocerebrosidase mutations in clinical and pathologically proven Parkinson's disease. *Brain*, **132**, 1783–1794.
48. Nishioka, K., Vilarino-Guell, C., Cobb, S.A., Kachergus, J.M., Ross, O.A., Wider, C., Gibson, R.A., Hentati, F. and Farrer, M.J. (2010) Glucocerebrosidase mutations are not a common risk factor for Parkinson disease in North Africa. *Neurosci. Lett.*, **477**, 57–60.
49. Ichimura, Y. and Komatsu, M. (2011) Pathophysiological role of autophagy: lesson from autophagy-deficient mouse models. *Exp. Anim.*, **60**, 329–345.
50. Panasyuk, G., Nemazanyy, I., Zhyvoloup, A., Filonenko, V., Davies, D., Robson, M., Pedley, R.B., Waterfield, M. and Gout, I. (2009) mTORbeta splicing isoform promotes cell proliferation and tumorigenesis. *J. Biol. Chem.*, **284**, 30807–30814.

51. Vitari, A.C., Deak, M., Collins, B.J., Morrice, N., Prescott, A.R., Phelan, A., Humphreys, S. and Alessi, D.R. (2004) WNK1, the kinase mutated in an inherited high-blood-pressure syndrome, is a novel PKB (protein kinase B)/Akt substrate. *Biochem. J.*, **378**, 257–268.
52. Nembrini, C., Kisielow, J., Shamshiev, A.T., Tortola, L., Coyle, A.J., Kopf, M. and Marsland, B.J. (2009) The kinase activity of Rip2 determines its stability and consequently Nod1- and Nod2-mediated immune responses. *J. Biol. Chem.*, **284**, 19183–19188.
53. Meylan, E. and Tschopp, J. (2005) The RIP kinases: crucial integrators of cellular stress. *Trends Biochem. Sci.*, **30**, 151–159.
54. Li, X., Wang, Q.J., Pan, N., Lee, S., Zhao, Y., Chait, B.T. and Yue, Z. (2011) Phosphorylation-dependent 14-3-3 binding to LRRK2 is impaired by common mutations of familial Parkinson's disease. *PLoS ONE*, **6**, e17153.
55. Deng, X., Dzamko, N., Prescott, A., Davies, P., Liu, Q., Yang, Q., Lee, J.D., Patricelli, M.P., Nomanbhoy, T.K., Alessi, D.R. *et al.* (2011) Characterization of a selective inhibitor of the Parkinson's disease kinase LRRK2. *Nat. Chem. Biol.*, **7**, 203–205.
56. Dzamko, N., Deak, M., Hentati, F., Reith, A.D., Prescott, A.R., Alessi, D.R. and Nichols, R.J. (2010) Inhibition of LRRK2 kinase activity leads to dephosphorylation of Ser(910)/Ser(935), disruption of 14-3-3 binding and altered cytoplasmic localization. *Biochem. J.*, **430**, 405–413.
57. Funayama, M., Hasegawa, K., Ohta, E., Kawashima, N., Komiyama, M., Kowa, H., Tsuji, S. and Obata, F. (2005) An LRRK2 mutation as a cause for the parkinsonism in the original PARK8 family. *Ann. Neurol.*, **57**, 918–921.
58. Jaleel, M., Nichols, R.J., Deak, M., Campbell, D.G., Gillardon, F., Knebel, A. and Alessi, D.R. (2007) LRRK2 phosphorylates moesin at threonine-558: characterization of how Parkinson's disease mutants affect kinase activity. *Biochem. J.*, **405**, 307–317.
59. Anand, V.S., Reichling, L.J., Lipinski, K., Stochaj, W., Duan, W., Kelleher, K., Pungaliya, P., Brown, E.L., Reinhart, P.H., Somberg, R. *et al.* (2009) Investigation of leucine-rich repeat kinase 2 : enzymological properties and novel assays. *FEBS J.*, **276**, 466–478.
60. Ohta, E., Katayama, Y., Kawakami, F., Yamamoto, M., Tajima, K., Maekawa, T., Iida, N., Hattori, S. and Obata, F. (2009) I(2020)T leucine-rich repeat kinase 2, the causative mutant molecule of familial Parkinson's disease, has a higher intracellular degradation rate than the wild-type molecule. *Biochem. Biophys. Res. Commun.*, **390**, 710–715.
61. Tucker, K.L., Wang, Y., Dausman, J. and Jaenisch, R. (1997) A transgenic mouse strain expressing four drug-selectable marker genes. *Nucleic Acids Res.*, **25**, 3745–3746.
62. Schwenk, F., Baron, U. and Rajewsky, K. (1995) A cre-transgenic mouse strain for the ubiquitous deletion of loxP-flanked gene segments including deletion in germ cells. *Nucleic Acids Res.*, **23**, 5080–5081.